International Journal of Thermal Sciences 200 (2024) 108989

Contents lists available at ScienceDirect

International Journal of Thermal Sciences

journal homepage: www.elsevier.com/locate/ijts

Experimental investigation for the loop heat pipe with a bifacial flat evaporator

Tingting Wang [a], Jing Zhao [a], Wei Liu [a], Lei Ma [b], Zhichun Liu [a,*]

[a] School of Energy and Power Engineering, Huazhong University of Science and Technology, Wuhan 430074, China
[b] Coll New Mat & New Energies, Shenzhen Technology University, Shenzhen 518118, China

ARTICLE INFO

Keywords:
Flat-type LHP
Two wicks
Bifacial heat load
Bimetal wall evaporator

ABSTRACT

To improve dual heat source cooling in a compact space, we designed a dual wick flat-type LHP with a bifacial evaporator, analyzed the evaporator's heat transfer process, and determined the impact of side-wall and backward conduction on system operation. To reduce side-wall conduction, the proposed LHP system uses a composite evaporator with a copper heating surface and a stainless steel shell. We tested start-up and variable heat load operation characteristics with one-side and bifacial heat loads. Theoretically, we analyzed the phenomena occurring in start-up and variable load processes. When heating the bottom heating surface, our innovative LHP could start and operate satisfactorily with a single-sided heat load of 10–160 W, according to the findings of the test. When only heating the top heating surface at a lower heat load, the system startup was not easy, but this problem could be improved by adjusting the heat load on the bottom heating surface. The highest one-side heat load was 80 W when the evaporator wall temperature was below 80 °C, and the heat flux at this time was equal to 16.63 W/cm^2. As for the heat load loaded on the upper and lower walls of the evaporator simultaneously, the maximum heat transfer was 80–80 W. This study provides guidance for LHPs' follow-up research and practical applications.

1. Introduction

LHP is a phase-change heat transfer device with high efficiency. Due to its numerous benefits, including low heat transfer resistance, high heat transfer efficiency, flexible layout, long transmission distance, light weight, and compact dimension, LHPs are considered to be widely used in electronic cooling and thermal management [1–5]. Their application in battery thermal management systems has received more and more attention.

Various authors [6–9] conducted experimental studies on the longitudinal liquid-supply-type and the ultra-thin-type LHPs used in battery thermal management systems. Zhang et al. [6,7] constructed a longitudinal, liquid-supply, flat-plate LHP system for heat dissipation within a limited space and thinned the evaporator wall to 8 mm. They tested the impacts of different condenser positions on system performance and studied the mechanism of the fluctuation phenomenon during the operation process. Hong et al. [8,9]produced multiple sets of ultra-thin LHP systems (1.5 mm) for the thermal management of battery systems. The evaporator was welded by two copper cover plates, one with thicknesses of 0.5 mm and 1 mm, respectively. The evaporator was engraved with many microgrooves. The influences of the inlet length, groove structure, condenser position, and inclination angle of the system were tested on the operating temperature, thermal resistance, and start-up characteristics. The heat load range of the test was 20–80 W. The results proved that the Ultra-thin LHP system could meet the battery's heat dissipation requirements. The system performance was optimal when the channel shape was a parallelogram and the operating temperature was lower than 50 °C. Other scholars have researched the application of LHP in the thermal management of automotive batteries. Aono et al. [10] designed a steady-state numerical model containing a two-phase flow pattern of the condenser to guide the development of an LHP with kW-class heat transport capability, which can transfer heat up to 6200 W under water cooling. Hashimoto et al. [11] proposed a new concept of LHP as a battery heating device for electric vehicles and conducted a temperature test on a simulated battery at a low temperature of −20 °C. The experimental results showed that the temperature of the simulated battery block reached more than 0 °C. The LHP could be used as a heating device for electric vehicle batteries in −20 °C environments. Bernagozzi et al. [12] proposed an innovative 3-cell battery module thermal management system to improve the key issues of

* Corresponding author.
E-mail addresses: malei@sztu.edu.cn (L. Ma), zcliu@hust.edu.cn (Z. Liu).

https://doi.org/10.1016/j.ijthermalsci.2024.108989
Received 11 April 2022; Received in revised form 9 October 2023; Accepted 22 February 2024
Available online 29 February 2024

electric vehicles. The experimental results showed that the system met the thermal requirements of the pack and cell level of the vehicle battery and could transfer 150 W of heat from the battery module to a remote heat exchanger connected to the vehicle's HVAC cooler, reducing the maximum temperature after rapid charging by 3.6 °C. Phan et al. [13] designed a dual flat-evaporator LHP with a capillary wick made of hydrophilic polytetrafluoroethylene porous membrane and a working fluid of water. Two flat evaporators were arranged on the upper and lower sides of the heat source. The system can maintain the heat source temperature below 130 °C in six typical directions.

In practice, heat-collecting plates are used to gather the scattered heat sources for heat management. However, when the electronic device structure is tightly arranged, the collector plate cannot occupy a large space. Scholars propose a multi-evaporator structure LHP system to deal with the problem of multi-heat-source dissipation [14–17]. The evaporators are arranged in parallel or in series. These two arrangements complicate the heat dissipation system's structure, making it challenging to ensure the stability and reliability of operation.

Multiple heat sources exist in the flat-panel fuel cell stack's heat source, and the structure is compact. In this case, a multi-evaporator heat dissipation system with a complex structure has poor applicability. Therefore, to solve the cooling issues of the fuel-cell-stacks-type flat-plate heat sources, some scholars proposed the LHP system with a two-wick evaporator. Chen et al. [18] developed a stainless steel-ammonia LHP that used two biporous wicks in the evaporator. The experiments' findings show that the capillary wick's porosity affects its thermal and hydraulic properties. The LHPs respond quickly and smoothly to heat loads and work consistently without oscillation. Liu et al. [19] designed a dual-wick FLHP system. They studied the innovative LHP's operation performance and discovered a practical method for increasing its operating capacity. The start-up and operation under variable heat loads were tested. The testing findings demonstrated that the new LHP was capable of starting and operating satisfactorily throughout a large heat load range (10 W–170 W). Wang et al. [20] studied the heat leaking influence on the dual-wick FLHP's compensation chamber. In the experiment, the maximum operating heat load was 210 and 270 W, respectively, with slopes of 10° and 90° when the heating surface temperature of the evaporator was below 90 °C. This system could be started successfully at 10 W, while comparable systems with a single wick would fail under this heat load. The system performed better in terms of temperature reduction and thermal resistance reduction when the back and wall of the evaporator were both heated.

For existing two-wick evaporators, when heat loads are simultaneously loaded on two heating surfaces, the capillary wick and the sidewall conduct a large quantity of heat to the compensation chamber. Then the working fluid in the compensation chamber gets easily

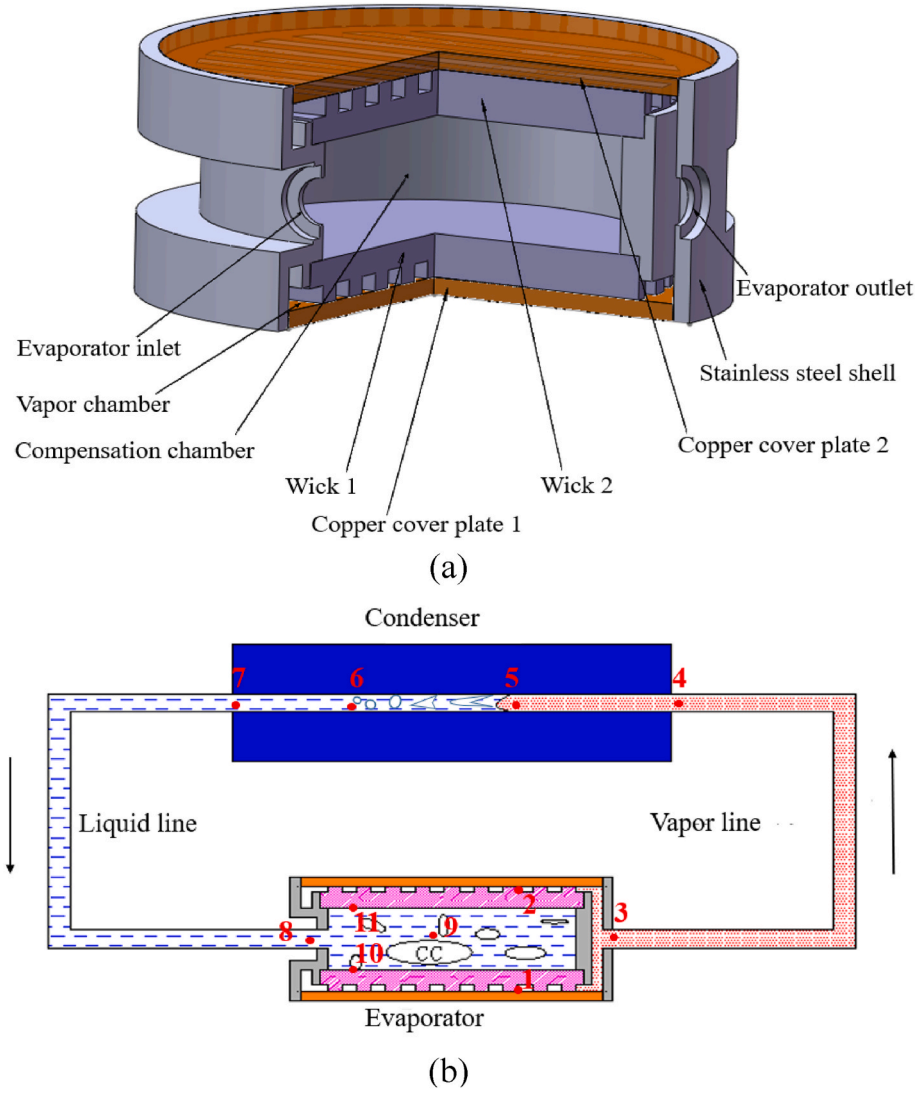

Fig. 1. Sketch maps of the two-wick FLHP system with composite evaporator: (a) Schematic of the two-wick evaporator; (b) Schematic of the overall structure of the LHP system.

vaporized and exists in a state of vapor and liquid coexistence. To solve this problem, in this study, we created a new structure for a two-wick composite evaporator LHP system. The heating surface is composed of copper, which has high thermal conductivity, and the material of the whole body is stainless steel with low thermal conductivity. The layout of the transmitted pipelines is flexible and can simultaneously control two heat sources. Most importantly, the composite evaporator can effectively suppress the heat conduction of the sidewall to improve the heat transfer capacity, temperature uniformity, reliability, and stability of the system. We analyzed the operation mechanism by studying the LHP performance at start up and variable heat load process, laying the foundation for follow-up research on two-wick LHPs and multi-evaporator LHPs.

2. Experimental setup

As shown in Fig. 1(a), we configured a new structure of a two-wick evaporator with a bimetal wall. The stainless-steel evaporator was equipped with two copper cover plates and two ribbed capillary wicks. The sintered nickel powder capillary wicks 1 and 2 about the evaporator's upper and lower surfaces. After internal compression, the copper cover plate and stainless steel body were welded to seal the evaporator. To avoid affecting the compensation chamber temperature, channels were used to link the top and bottom vapor chambers in this experiment. Fig. 1(b) shows the system's overall structure. A tube-to-tube heat exchanger was designed as the condenser, and the refrigerant was a 50% mass fraction of ethylene glycol solution. We used a stainless-steel pipe as the transmission pipeline.

Fig. 2 depicts the thermodynamic diagram for the two-wick LHP system with identical heat loads on both sides. Each state point has corresponding positions in Fig. 1(b). The saturation line's state points 1 and 2 correspond to the vapor side of the bottom and top wicks' vapor-liquid interfaces, respectively. Point 3 is the state of the working fluid at the evaporator outlet. Flow loss happens when the vapor produced by the wick passes through the vapor channel and the vapor continues to be heated by the heating surface. The working fluid is now superheated, then it enters the condenser through the vapor pipeline. In an ideal state, the working fluid at point 4 is in a superheated state, or it may be in a two-phase state. The working fluid condenses in the condenser and finally becomes a supercooled liquid, which experiences three states: the superheating state (4–5), the two-phase state (5–6), and the supercooling state (6–7). The supercooled liquid flows back to the compensation chamber through the liquid pipeline and dissipates heat to the environment or absorbs heat from the environment simultaneously. The working fluid is set to enter the compensation chamber at point 8. After entering the compensation chamber, the working fluid changes from a supercooled state to a saturated state 9. The vapor-liquid interface's liquid characteristics at the capillary wick's bottom and top are determined by points 10 and 11 on the saturation line, respectively. The working fluid is heated when it flows through the capillary wick. The pressure at point 10 is higher than that at point 11 due to gravity's action. The gasification of the working fluid via the bottom and top wicks is seen in Sections 1-10 and 2-11, respectively.

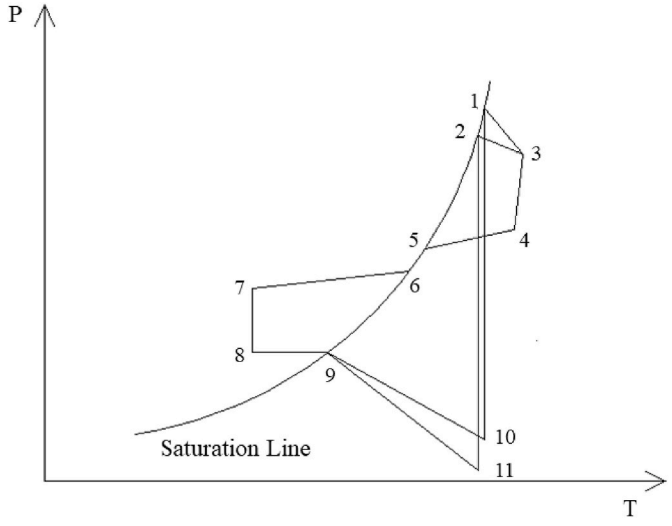

Fig. 2. Thermodynamic diagram of two-wick LHP system.

The thickness of the stainless steel shell and the copper cover were both 1.5 mm. In order to avoid the evaporator occurrence of larger deformation, the strength analysis was conducted via Ansys software. The strength and deformation rate calculation results are presented in Fig. 3. The experiments could be performed within the safety range and ensure there will be no large deformation for the evaporator.

The experimental system was filled with methanol as the working fluid, and the filling ratio was 69%. We emptied the LHP system to 3×10^{-4} Pa before charging the working fluid. The experimental system's primary structural parameters are provided in Table 1. To reduce the operating temperature of the system and make it easier to startup, we designed an experiment to test the system's operation characteristics at a tilt angle of 10° (as shown in Fig. 4). The angle remained constant throughout the experiment. In our study, the copper cover plate at the bottom of the evaporator was called heating surface 1. The capillary wick next to it was called wick 1. The copper cover plate at the top of the evaporator was labeled heating surface 2, and the relevant wick was called wick 2. The heating loads applied to each surface were Q1 and Q2, respectively.

The T type of thermocouple was used to monitor the temperature variation during the LHP system operation, and the mounting positions were shown in Fig. 5. Three thermocouples (TC1, TC2, and TC3) were connected to the vapor line to measure the temperature of the evaporator outlet ($T_{e\text{-}o}$), the vapor line, and the condenser inlet ($T_{c\text{-}i}$), respectively. Similarly, for the liquid line, TC7, TC8, and TC9 were used to monitor the temperature changes of the liquid working fluid in the liquid line. TC6 and TC10 were respectively attached to the condenser outlet ($T_{c\text{-}o}$) and evaporator inlet ($T_{e\text{-}i}$). Four thermocouples were arranged on the walls of heating surface 1 (T_{e1}) and heating surface 2 (T_{e2}), respectively, and their average values were taken as the temperatures of each heating surface. TC20 and TC21 were connected to the evaporator's side wall to characterize the compensation chamber's temperature (T_{cc}). TC4 and TC5 were respectively connected to the outlet and inlet of the coolant. T19 was used to measure ambient temperature (T_{amb}). The experimental system and methods were consistent with ref. 17 [21].

3. Results and discussion

3.1. Start-up characteristics

The minimum heat load required for LHP system startup is called the threshold. System failure occurs if the heat load is below the threshold. If the threshold is too high, the application of the LHP will be restricted. Start-up is a highly complex process. Numerous variables affect the start-up characteristics of LHP, including heat load, system attitude (the relative position relationship between the evaporator and condenser), and heat sink temperature. Research on the start-up performance of LHP is important for improving the effective operating range of LHP.

3.1.1. Start-up characteristics with single-side heat load

In the experiment, we investigated the start-up procedure of a two-wick bifacial evaporator LHP system with a single-side heat load.

Fig. 6 illustrates the start-up curve when just heating surface 1 was subjected to the heat load. The system could be started with a heat load of 10–160 W when the heat source temperature was lower than 80 °C. Three types of start-up modes were observed during the start-up process.

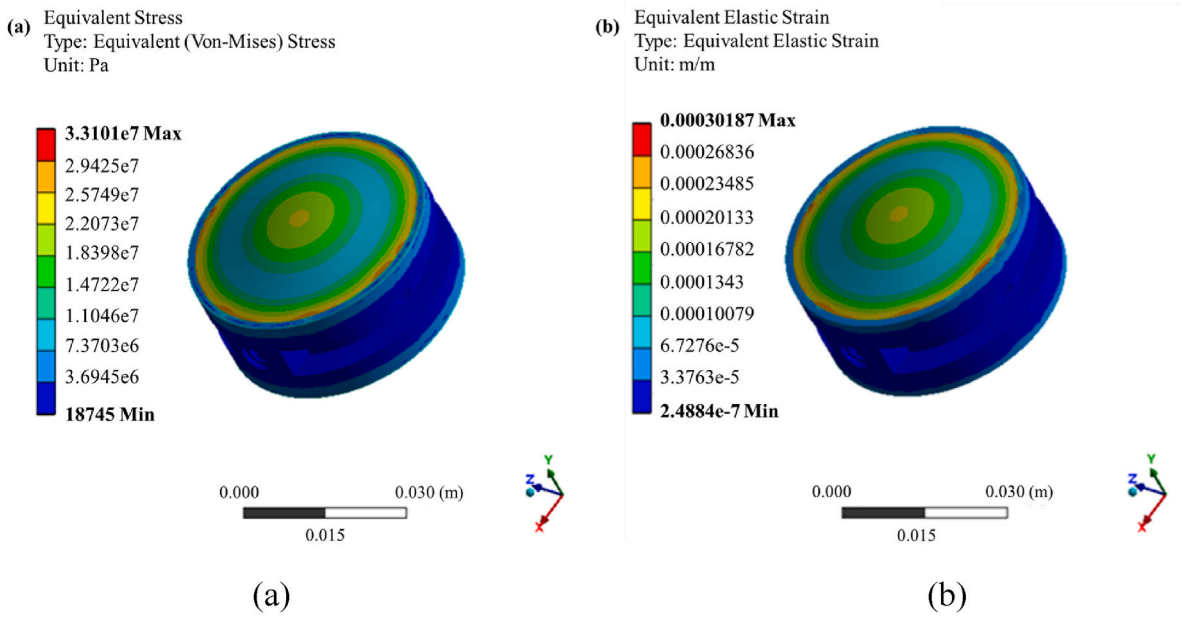

Fig. 3. Strength check (a) and deformation rate (b) of the composite evaporator.

Table 1
Geometric characteristics of the LHP system.

Evaporator	Wick 1	Diameter (mm)	37	Vapor line	Inner diameter (mm)	4
		Thickness (mm)	3.5		Length (mm)	220
		Porosity (%)	75	Liquid line	Inner diameter (mm)	4
	Wick 2	Diameter (mm)	37		Length (mm)	340
		Thickness (mm)	3.5	Condenser	Diameter (mm)	4
		Porosity (%)	75		Length (mm)	600
	Compensation chamber	Outer diameter (mm)	34			
		Thickness (mm)	10			

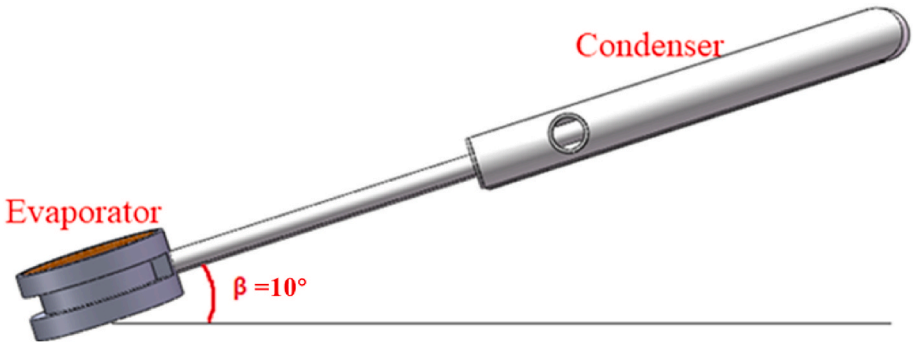

Fig. 4. Set up of the system during the test.

The working fluid circulation in the system was discontinuous at low heat loads. As a result, the start-up curve showed fluctuations (Fig. 6(a, b)), and the system needed a long time to start. When the heat load increased, the compensation chamber experienced a continual backflow of the supercooled liquid. However, the mass flow rate was low. Under these circumstances, the start-up curve was stepped (Fig. 6(c,d)). After a particular degree of heat load had been reached, the working fluid circulated significantly. Therefore, the supercooled liquid flowed back quickly, and the system started and stabilized in a short time (Fig. 6(e, f)).

The stepwise start-up of the system showed two alternative modes, as illustrated in Fig. 6(c and d). When the heat load was 30 W, the temperatures of heating surface 1 and the compensation chamber were characterized by a peak-like behavior known as overshoot. This occurred because the vapor channel was in a liquid form when the system was cold, and the working fluid needed a certain degree of superheat to vaporize. The temperatures of heating surface 1 and the compensation chamber grew dramatically over this time. The cumulative pressure of the gaseous working fluid grew as the working fluid in the vapor channel evaporated, and the working fluid began to flow. When the temperatures of the evaporator outlet and the condenser inlet rose sharply, and the temperatures of heating surface 1 and the compensation chamber dropped rapidly, the working fluid began to circulate in the loop. The compensation chamber cooled, and the operating temperature curve had a sharp peak. When the compensation chamber reached an energy equilibrium, the LHP system became stable. The working fluid in the vapor channel already existed in a gaseous form before startup with a 40 W heat load. When the heating surface was

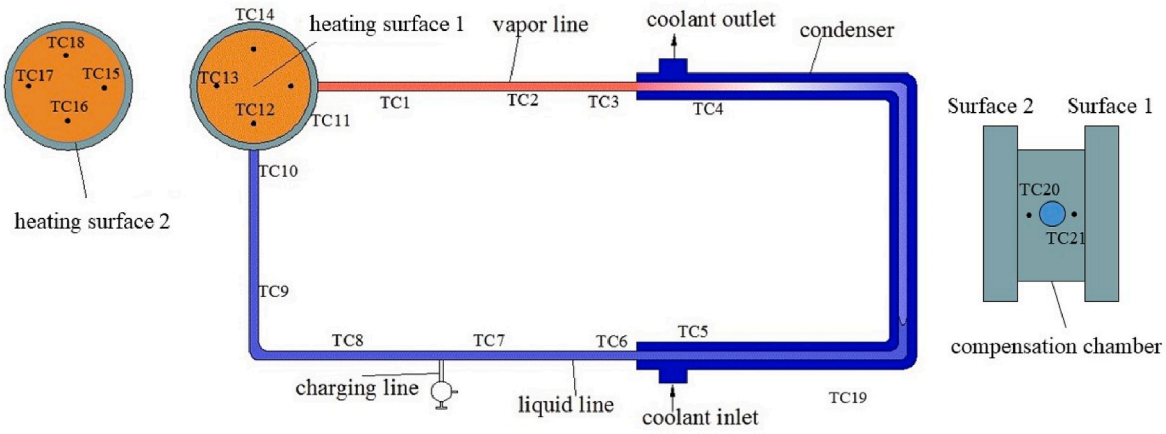

Fig. 5. Schematic diagram of thermocouple layout position.

subjected to a heat load, vaporization occurred quickly in the vapor channel, and the heat was removed. Thus, there was no peak phenomenon during the start-up.

As shown in Fig. 6(a and b), we observed the overshoot phenomenon in the early stage of the 10 W and 20 W start-up process, consistent with the overshoot phenomenon observed at 30 W start-up. The temperatures of heating surface 1 and the compensation chamber increased quickly. The outlet temperature was less than the compensation chamber temperature. The condenser inlet temperature abruptly increased after a period of time. The temperatures of heating surface 1 and the compensation chamber subsequently dropped. The working fluid began to circulate, and the overshoot phenomenon appeared; this was also caused by the vapor channel being filled with liquid when the system was in a cold state. As shown in Fig. 6(f), the vapor channel was also full of liquid before the start-up process at 140 W, but the system started quickly owing to the high heat load, and the overshoot phenomenon was not apparent.

Fig. 7 depicts heating surface 2's performance under a 20 W heat load. At the initial heating stage, the temperatures of heating surface 2, compensation chamber, and heating surface 1 increased owing to heat conduction. The evaporator outlet temperature also increased at a constant rate, which indicated the liquid working fluid in the wick was constant. When vapor channel pressure increased, the working fluid flowed, and the operating temperature decreased. The temperatures of heating surface 2, the compensation chamber, the evaporator outlet, and heating surface 1 continued to rise, and the system failed to start.

For heating surface 2, the vapor channel was located above the compensation chamber and the liquid supply of the fluid from the compensation chamber to the capillary wick needed to overcome gravity. The absorbing surface of wick 2 was being blocked by vapor in the two-phase state of the working fluid in the compensation chamber. Therefore, the startup failure of surface 2 might be due to the insufficient liquid supply to the capillary wick, and the working medium could not be continuously sucked by the capillary wick to the phase transition interface.

In addition, the reason for system startup failure might also be due to the excessive thermal resistance of the evaporator. The evaporator's heat load was divided into three parts: Q_a, heat transfer from the evaporator sidewall to the compensation chamber wall, Q_b, heat conduction through the heating surface and the rib to the gas-liquid interface of the capillary wick, and Q_c, heat for liquid vaporization. Q_b accounted for the most significant proportion. The working fluid in the capillary wick absorbed Q_b to vaporize, and the vapor pressure promoted the working fluid circulation. The evaporator's thermal resistance affected Q_b. If the thermal resistance was large, the amount of vaporization in the capillary wick would be small, and Q_a would be large. The compensation chamber temperature and pressure increased, and the pressure differential between the wick's vapor-liquid interface and the compensation chamber was inadequate. The system's working fluid could not circulate, impeding the heat removal, the heating surface temperature continued to rise, and the system failed to start up.

The evaporator thermal resistance is defined as the ratio of the difference in temperature between the evaporator wall and the vapor temperature at the evaporator outlet to the heating load. It is divided into three parts: thermal resistance of the heating cover plate, contact thermal resistance between the cover plate and capillary wick, and thermal resistance of vaporization. The heating cover plate was determined by the material and size of the cover. The working fluid transferred heat through a phase change, and the thermal resistance of vaporization was low. Therefore, we inferred that the evaporator's high thermal resistance was produced by the evaporator's high contact thermal resistance, which was caused by the cover plate's inadequate contact with the capillary wick. The quality of the capillary wick, the precision with which the cover plate was processed, and the welding method used on the evaporator all had an effect on the contact thermal resistance. Meanwhile, due to insufficient liquid supply to the capillary wick, the wettability of the capillary wick was poor, and the contact between the capillary wick and the cover plate was prone to forming a cavity to store noncondensable gases, further increasing the contact thermal resistance.

Fig. 8 shows that when Q_2 was 30 W, the working fluid in wick 2 vaporized, and the evaporator outlet temperature increased slowly. The compensation chamber temperature and pressure rose as a result of the considerable side-wall conduction. The system proved difficult to start up because the vapor-liquid interface and the compensation chamber had insufficient pressure differential for the working fluid to flow. When we increased Q_1 to 50 W, the working fluid in capillary wick 1 absorbed heat and then vaporized. The gaseous working fluid entered the condenser, increasing the condenser inlet temperature. Additionally, the gaseous working fluid condensed into a supercooled liquid, which acted as a heat transfer medium for the cooling system. Subsequently, the evaporator inlet temperature decreased. The supercooled liquid was returned to the compensation chamber, the evaporator cooled, each testing point's temperature lowered, and the operation finally stabilized. The amount of vaporized working fluid in wick 2 was small. However, the system's circulation was pushed by the working fluid generated in wick 1. The heat of heating surface 2 was continuously removed, so the final temperature was stable.

Fig. 9(a) depicts the operating curve when the system was started while keeping $Q_1 = 60$ W unchanged and gradually increasing Q_2. At the beginning of the test, when $Q_1 = 60$ W, the system overshot; we increased Q_2 to 10 W after the system was stable. Because of the inadequate heat dissipation of heating surface 2, the compensation chamber was heated, and the operating temperature of heating surface 1 rose. The

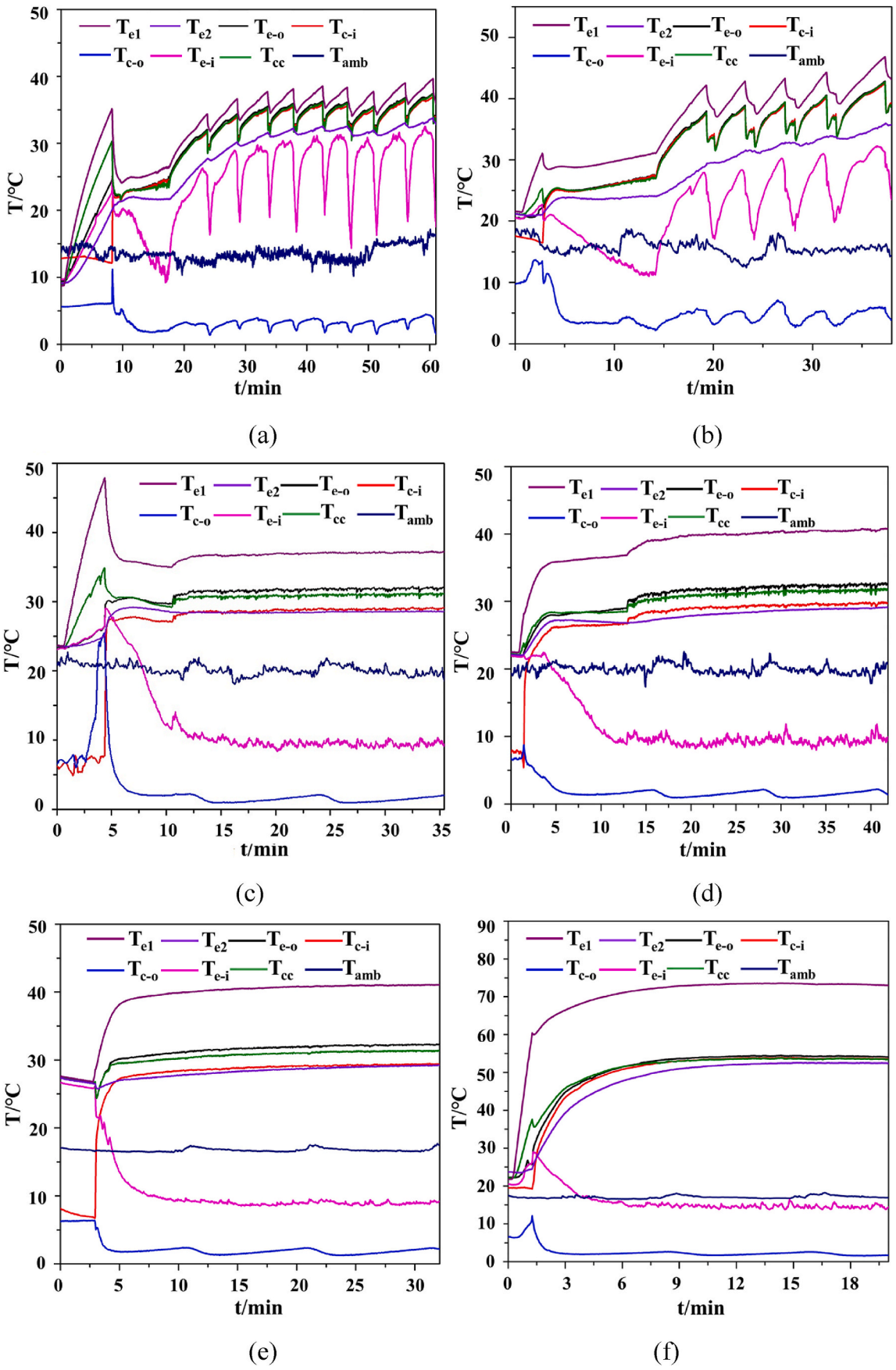

Fig. 6. The LHP's start-up performance when Q1 was 10 (a), 20 (b), 30 (c), 40 (d), 50 (e), and 140 W (f).

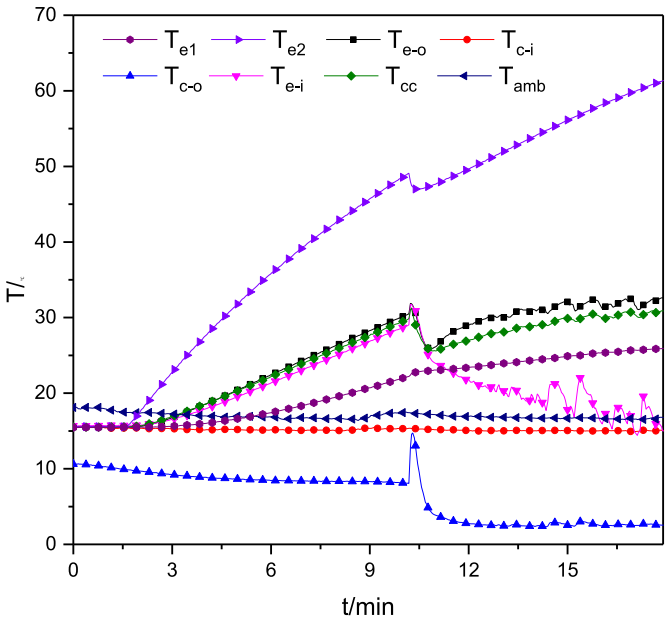

Fig. 7. The LHP's start-up performance when Q_2 was 20 W.

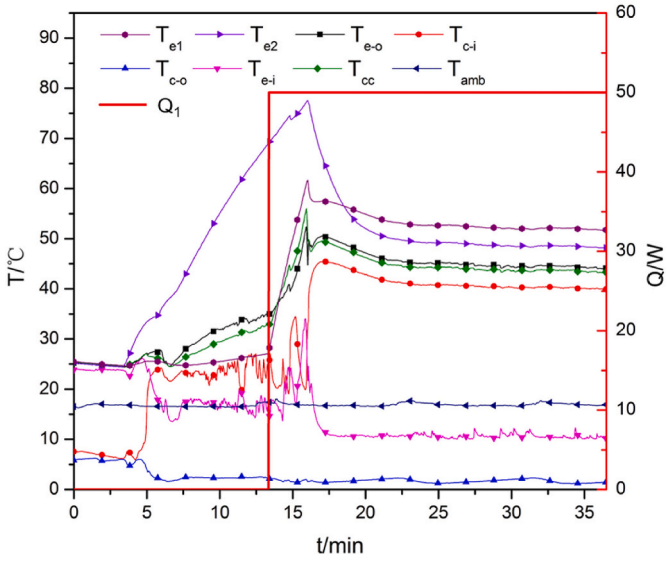

Fig. 8. The LHP's startup performance when Q_2 = 30 W.

heat of heating surface 2 was removed by the continuous circulation of the working fluid. Finally, the system reached stable energy. Therefore, the operating temperature was stable. When we increased Q_2, the temperatures of heating surfaces 1 and 2 rose and eventually reached a new energy equilibrium.

Fig. 9(b) shows the temperature difference between heating surfaces 1, 2 and the vapor outlet during the operation process. The phase change heat transfer of capillary wick 1 remained constant as Q_1 remained unchanged. Thus, the temperature difference between the heating surface 1 and the evaporator outlet did not change significantly after the start-up was stabilized. However, as Q_2 increased, the temperature difference slightly decreased because the working fluid circulation increased in the system. Heating surface 2 corresponded to an extended cooling surface, which had a lower temperature than the evaporator outlet. When the heat load was applied on heating surface 2, the temperature difference between the heating surface and the evaporator outlet became positive and increased as the heat load increased.

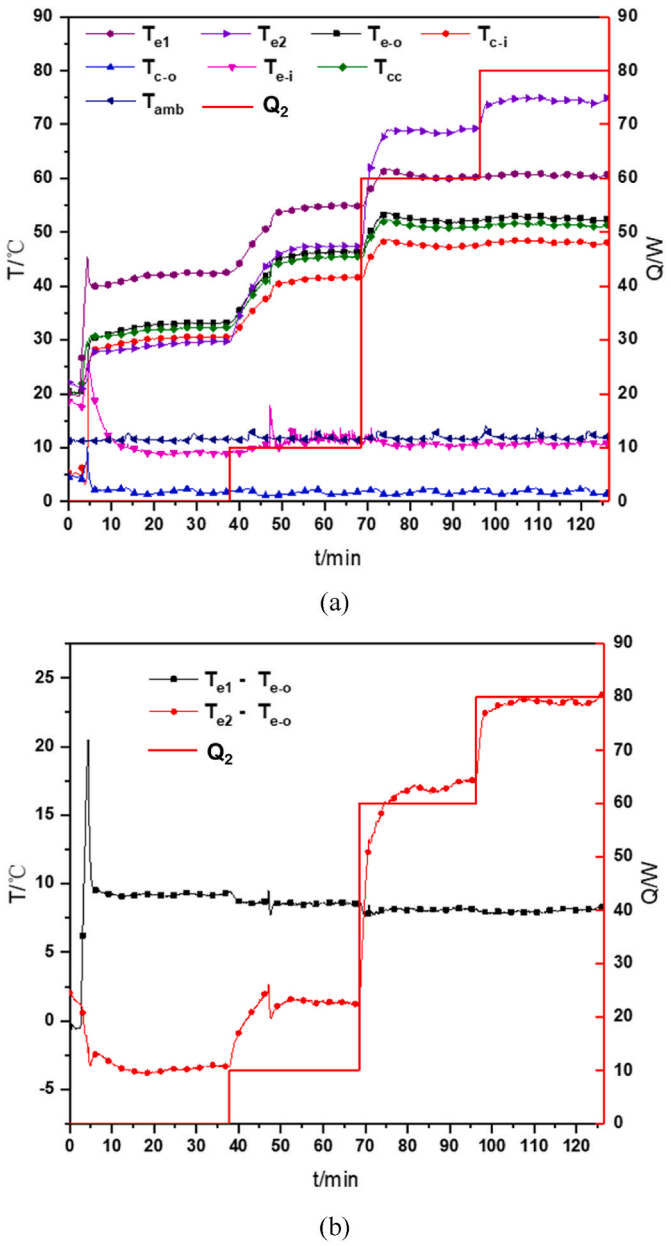

Fig. 9. (a) Temperature curve and (b) temperature difference for Q1 = 60 W and Q2 = 0–80 W.

3.1.2. *Start-up characteristics with both-side heat load*

We investigate the bifacial heat load startup procedure by providing heat to both heating surfaces of the LHP system.

In Fig. 10, the initial heat loads of the system were Q_1 = 10 W and Q_2 = 30 W. We observed a rise in the temperatures at the condenser inlet and compensation chamber. The temperature rise rate of heating surfaces 1 and 2 and the compensation chamber slowed, suggesting the working fluid circulation. However, the circulation was low, and the heat dissipation capacity was poor. When the heating surface temperature was raised to 70 °C, the operation was unstable. Increasing Q_1 to 30 W accelerated the vaporization of the working fluid in wick 1 and increased the heat dissipation capacity of the evaporator. The evaporator cooled when a substantial volume of supercooled liquid went back into the compensation chamber. The temperature decreased and finally entered a stable fluctuating state. By increasing Q_1, the working fluid circulation in the system could be improved, and fluctuations could be eliminated.

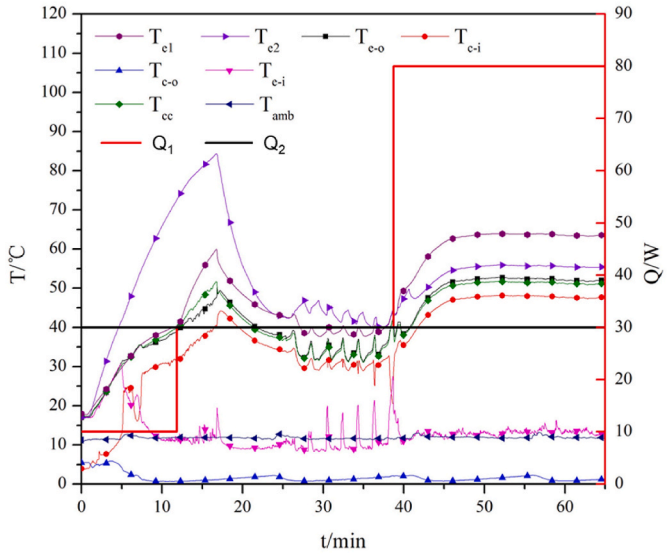

Fig. 10. The system's startup curve with $Q_2 = 30$ W and $Q_1 = 10$–80 W.

Fig. 11 depicts the start-up curve of the system when $Q_1 = 30$ W and $Q_2 = 50$ W. The system started smoothly at around 20 min. Under the circumstances, heating surface 1 had a lower heat load than heating surface 2, which was similar to Fig. 10. Because Q_1 and Q_2 increased, the system's working fluid vaporization rate was increased, and the rate of pressure rise in the vapor channel was more significant than that in the compensation chamber. The working fluid began to cycle up when the pressure difference was sufficient to overcome the system's flow resistance. The heating surface 1 temperature decreased, and the temperature rise rate of heating surface 2 decreased. As the flow gradually stabilized, the system became stable, and the temperature of each measuring point was constant.

Figs. 12 and 13 depict the start-up curve of the system when the two heating surfaces were supplied with the same heat load. As shown in Fig. 12, with heat loads $Q_1 = 10$ W and $Q_2 = 10$ W, during the early start-up period, the heating surface 1 temperature and the compensation chamber temperature rose rapidly, and the heating surface 2 temperature rose slowly. Upon increasing the heating surface 2 temperature, the

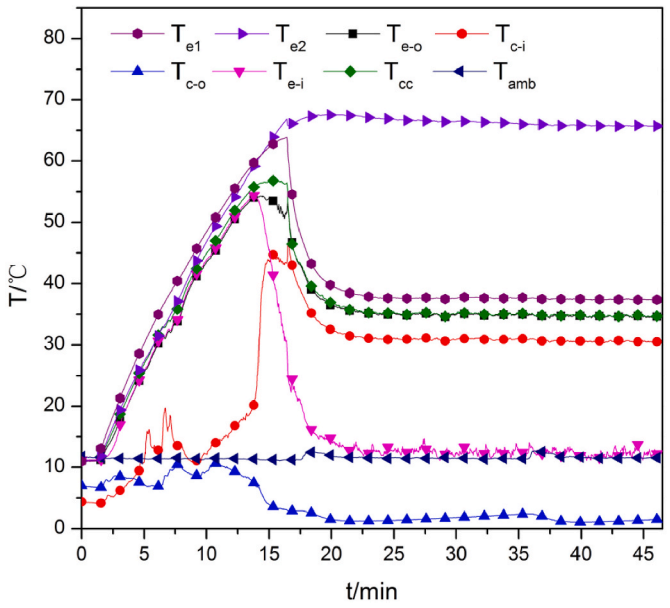

Fig. 11. The system's startup curve with $Q_1 = 30$ W and $Q_2 = 50$ W.

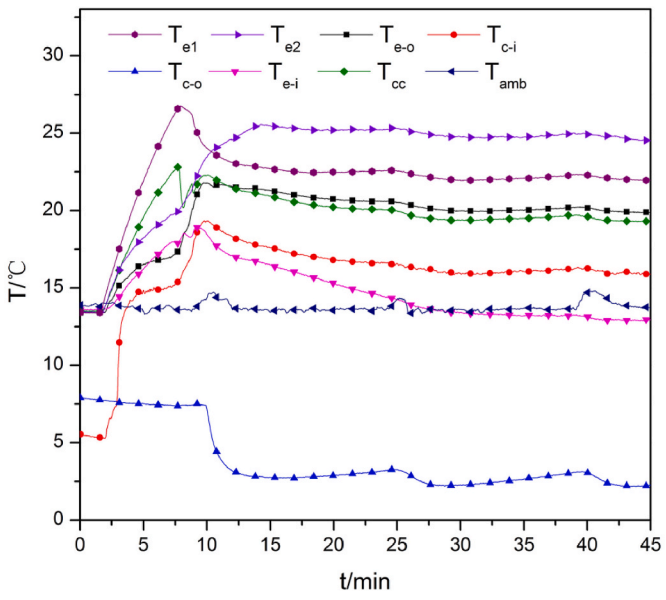

Fig. 12. The system's startup curve when $Q_1 = 10$ W and $Q_2 = 10$ W.

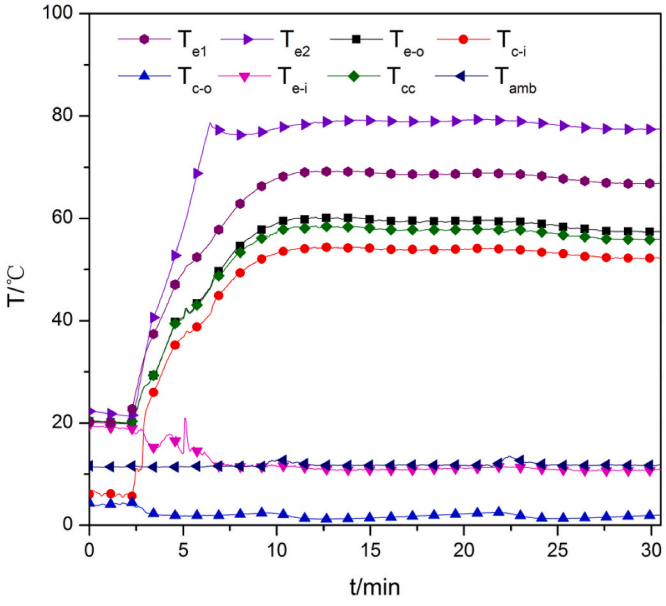

Fig. 13. The system's startup curve when $Q_1 = 80$ W and $Q_2 = 80$ W.

evaporator outlet temperature and condenser inlet temperature rose slowly, indicating that capillary wick 2 evaporated a little quantity of working fluid into the condenser and capillary wick 1 was lacking liquid. As time passed, the vapor pipeline pressure increased, and the system's working fluid started to flow. The condenser outlet temperature decreased, and the reflux liquid entered the compensation chamber. After reaching energy equilibrium, the system operated stably. As shown in Fig. 13, the start-up curve for the system when the heat load on both heating surfaces is raised to 80 W; it illustrates that the system can start fast and maintain a stable condition.

Because of the considerable contact thermal resistance between the capillary wick 2 and heating surface 2, the heating surface 2 temperature was greater when two heating surfaces were loaded with the same heat load. The system started faster and the temperature difference between the two heating surfaces increased with increasing heat load.

3.2. Operation with variable heat load

Fig. 14 shows the variable heat load operating curve when only surface 1 is heated. When the initial heat load of the system was 10 W, reaching the state of energy equilibrium and temperature stabilization took a long time. During this process, the condenser and evaporator outlet temperatures remained unchanged. When $Q_1 = 20$ W, the evaporator outlet temperature increased, and at the same time, the condenser outlet temperature decreased, indicating that when $Q_1 = 10$ W, no working fluid was circulating in the system, and the evaporator dissipated heat through heat conduction and remained stable. As the head load increased, the heating surface temperature rapidly increased, the pressure increased in the vapor channel, and the system's pressure equilibrium was destroyed, pushing the working fluid to flow. Under 20 W and 30 W heat loads, the system's working fluid circulation was unstable. As the heat load rose, the liquid content of the compensation chamber increased, and the system stability was enhanced without temperature fluctuations. When heating surface 1 was below 80 °C, the maximum heat load reached 160 W, equating to a 16.63 W/cm^2 heat flux.

Based on each stable stage of continuous operation, a schematic diagram of the relationship between operating temperature and heat load was drawn, as shown in Fig. 15. With 50 W as the boundary point, the entire process could be divided into two operating modes: variable conductance mode and constant conductance mode. When the heat load increased from 20 W to 50 W, the temperature difference between the condenser outlet and evaporator inlet decreased with the increased heat load, and the compensation chamber temperature reached its lowest point at 50 W. In this heat load range, the system was in variable conductance mode. When the heat load exceeded 50 W, the operating temperature increased linearly with the heat load, and the condensing surface in the condenser was fully opened. Thus, the condenser reached maximum condensation efficiency.

Fig. 16 shows the system's operating conditions when heating two heating surfaces simultaneously. The maximum heat load applied to a single heating surface was 80 W when the heating surface temperature was below 80 °C. Owing to the higher heat transfer resistance of heating surface 2, it operated at a higher temperature than heating surface 1. Compared to the single-sided heating in Fig. 15, the operating temperature of heating surface 1 was high when applying the same heat load on both sides. When Q_1 was 10 W and Q_2 was 0 W, the system was not in the phase-change heating mode. Therefore, the temperature was higher than that of the bifacial heating.

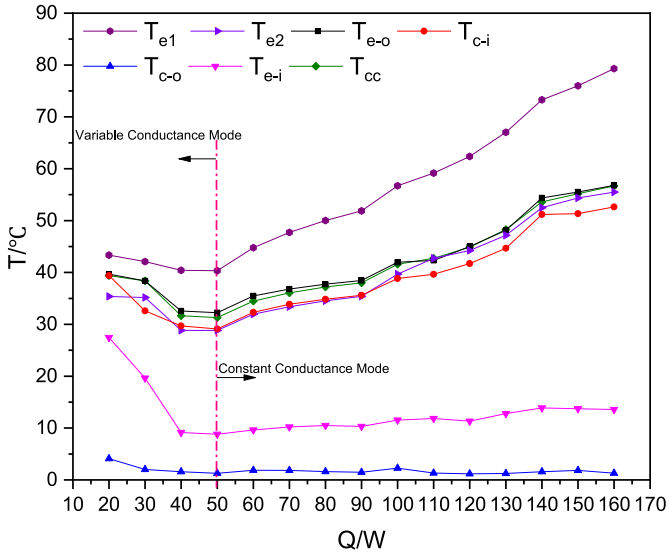

Fig. 15. The relationship between operating temperature and heat load.

3.3. Thermal resistance analysis

The thermal resistance of the system (R_{LHP}) and the thermal resistance for evaporation (R_{evap}) determine the LHP system's heat transfer performance. The formulas are as follows:

$$R_{LHP} = \frac{T_{e-wall} - T_{cond}}{Q} \tag{1}$$

$$R_{evap} = \frac{T_{e-wall} - T_{e-out}}{Q} \tag{2}$$

where Q denotes the heat load, $T_{e\text{-}wall}$ represents the evaporator wall's

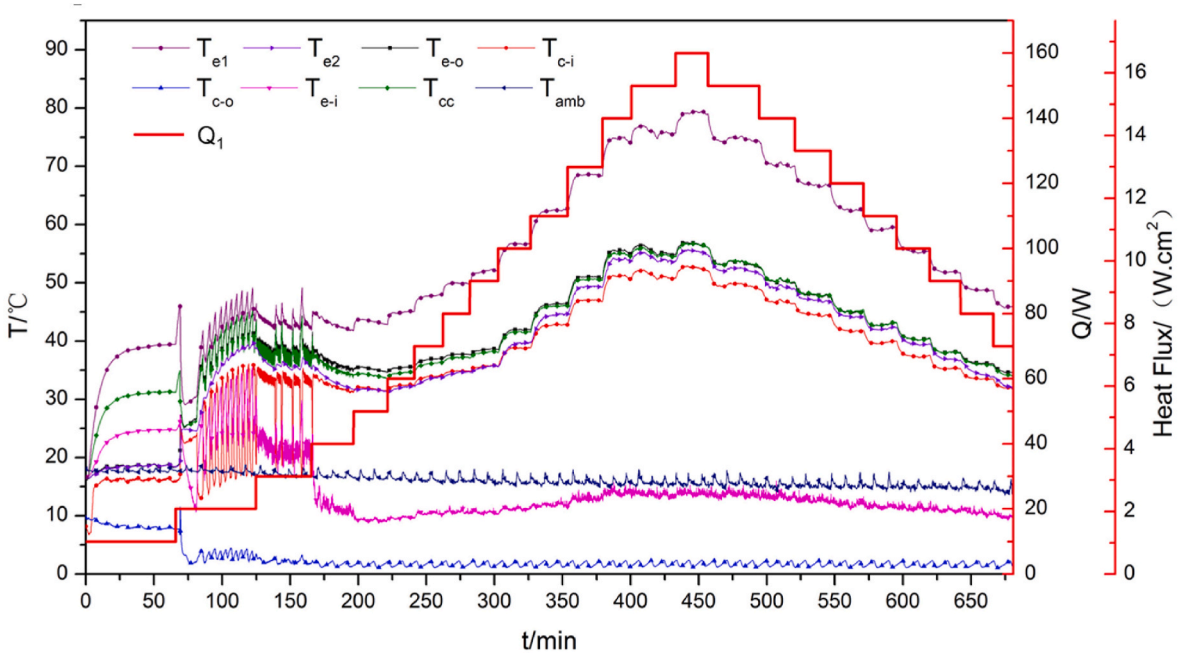

Fig. 14. The LHP's operating performance with variable heat loads on one side.

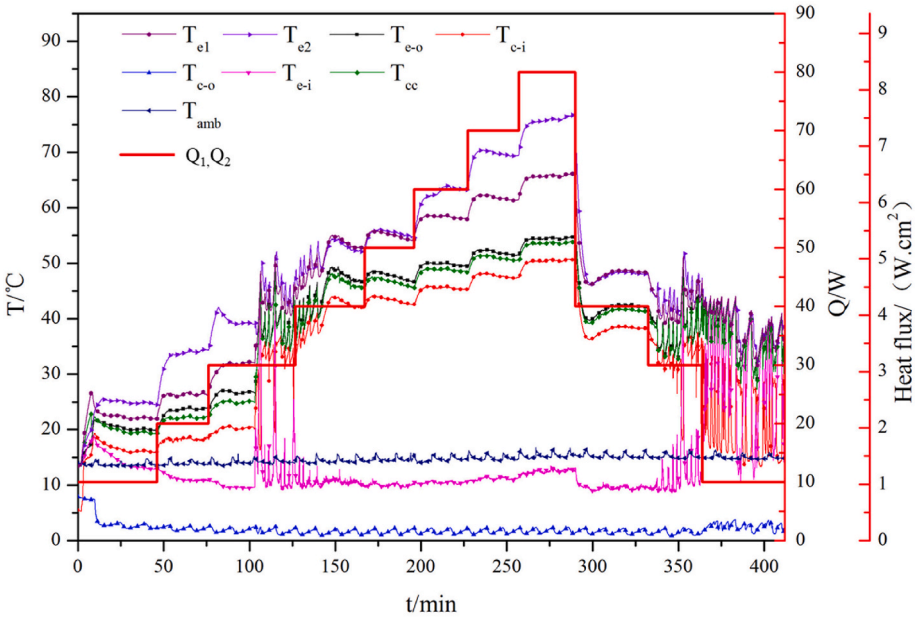

Fig. 16. The LHP's operating performance with variable heat loads on both side.

average temperature, T_{cond} denotes the condenser's average temperature and $T_{e\text{-}out}$ is the evaporator outlet temperature.

Fig. 17 shows the relationship between thermal resistance and heat load when only surface 1 was heated. The evaporator-to-condenser thermal resistance (R_{LHP}) and the evaporation thermal resistance (R_{evap}) gradually decreased as the heat load grew. When the heat flux was relatively low, the thermal resistance was greatly influenced by the heat load, as for higher heat flux, the effect was small. R_{LHP1} varied from 2.395 °C/W to 0.324 °C/W with a heat load of 10–160 W R_{evap1} remained basically unchanged when the heat load was greater than 80 W. When the heat load exceeded 30 W, R_{evap1} stabilized at 0.140 °C/W.

Fig. 18 shows the relationship between thermal resistance and heat load when equal heat load was applied to both sides. Both the loop thermal resistance and the evaporation thermal resistance decreased with the heat load increase. When the same heat load was applied to surfaces 1 and 2, the loop thermal resistance (R_{LHP2}) and the evaporator thermal resistance (R_{evaq2}) calculated by the wall temperature of heating surface 2 are higher than those calculated by the heating surface 1

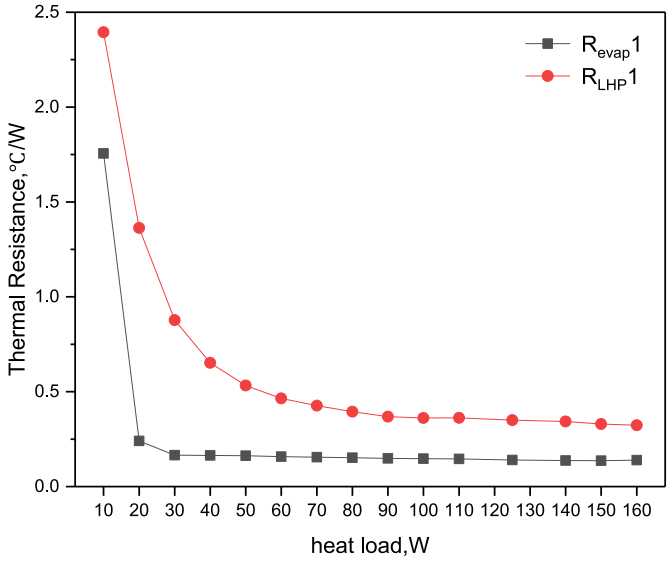

Fig. 17. Thermal resistance when only surface 1 was heated.

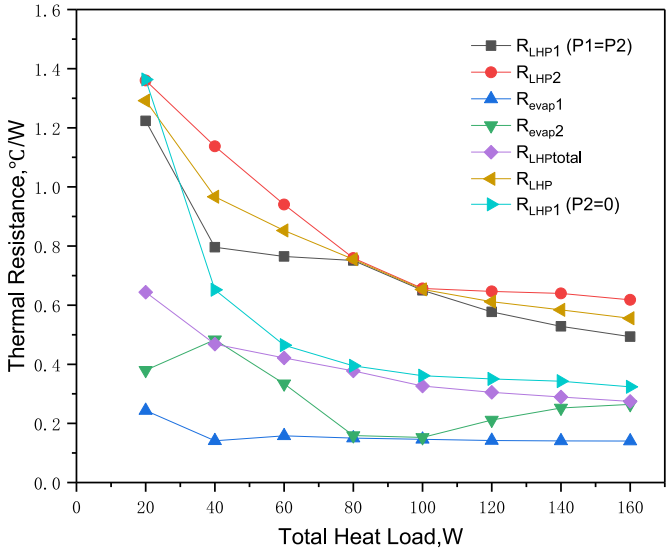

Fig. 18. Thermal resistance with bifacial heat load.

temperature. This was because the heating surface 2's heat transfer resistance was relatively large. With the same heat load, heating surface 2 had a higher operating temperature than heating surface 1. R_{LHP} was determined using the average of heating surfaces 1 and 2. Since R_{LHP1} and R_{LHP2} were relatively close, R_{LHP} can replace them equivalently. Upon the same heat load on heating surfaces 1 and 2, the generated vapor was collected in the vapor chamber and circulated through the common external loop. Based on the parallel resistance calculation principle, $R_{LHPtotal}$ can be calculated as follows. $R_{LHPtotal}$ varied from 2.395 °C/W to 0.324 °C/W with a heat load of 10–160 W.

$$R_i = \frac{T_{ei} - T_{cond}}{Q} \tag{3}$$

$$\frac{1}{R_{LHPtotal}} = \frac{1}{R_1} + \frac{1}{R_2} \tag{4}$$

where Q represents the heat load applied to heating surfaces 1 ($i = 1$)

and 2 ($i = 2$), T_{ei} represents the temperature of heating surfaces 1 and 2 ($i = 1,2$), T_{cond} is the condenser's average temperature, R_i is the loop thermal resistance corresponding to heating surfaces 1 and 2 ($i = 1,2$).

Fig. 18 also compares the R_{LHP1} of single-side heat load with R_{LHP1} of double-side heat load. Since Q_2 has an effect on the compensation chamber during double-sided heating, and the high temperature of the compensation chamber led to a high operating temperature of heating surface 1, R_{LHP1} with bifacial heat load was larger than that with the heat load applied to surface 1 only.

4. Conclusions

This study found that a two-wick LHP system with a bifacial evaporator is suitable for fuel cell flat heat sources. The evaporator had a bimetallic stainless steel–copper wall. We tested and analyzed the causes of different phenomena in the startup process. We also studied the variation law of operating temperature at various heat loads. The main results are as follows:

(1) Under the single-side heat load condition, heating surface 1 performed better. When heating surface 1 alone, the system could start properly in the 10–160 W heat load range. As the heat load gradually increased, we observed three start-up modes.
(2) Due to the need for counter gravity for the liquid supply of capillary wick 2, the wettability of capillary wick 2 was poor. We observed a considerable contact thermal resistance between heating surface 2 and capillary wick 2, resulting in a low heat transfer efficiency from heating surface 2 to capillary wick 2. The heat load strongly affected the compensation chamber, which could easily lead to start-up failure, operation failure, or system destabilization.
(3) When the heat load was applied on the upper and lower walls of the evaporator simultaneously. If the heat load Q_1 on heating surface 1 was lower than the heat load Q_2 on heating surface 2, the system would start with difficulty or even fail. By increasing Q_1, the circulation of the working fluid in the system increased, and temperature fluctuations could be eliminated. Therefore, the system could start successfully when Q_1 equals or exceeds Q_2. The system started quicker as the heat load increased. The system performed better at lower temperatures and thermal resistances.
(4) We tested the variable heat load operation when heating surface 1 alone. The system's maximum heat transfer was 160 W (16.63 W/cm^2) when the heating surface 1 temperature was lower than 80 °C. The maximum heat transfer was 80–80 W with the same heat load on both sides. The heat dissipation capacities of heating surfaces 1 and 2 deviated owing to the complexity and uncontrollability of the evaporator manufacturing process.
(5) The contact state between the heating surface and capillary wick determined the evaporator thermal resistance, directly affecting the LHP operation performance. We can improve the two-wick evaporator and reduce thermal resistance by optimizing the design and processing of the evaporator structure.

Declaration of competing interest

The authors claim that none of the material in the paper has been published or is under consideration for publication elsewhere.

Data availability

Data will be made available on request.

Acknowledgment

This work was supported by the National Natural Science Foundation of China (Grant No. 52076088) and the Core Technology Research Project of Shunde District, Foshan City, China (No. 2130218002932).

References

[1] R. Singh, A. Akbarzadeh, C. Dixon, M. Mochizuki, R.R. Riehl, Miniature loop heat pipe with flat evaporator for cooling computer CPU, IEEE Trans. Compon. Packag. Technol. 30 (1) (2007) 42–49.
[2] J.H. Boo, W.B. Chung, Experimental study on the thermal performance of a small-scale loop heat pipe with polypropylene wick, J. Mech. Sci. Technol. 19 (2005) 1052–1061.
[3] L. Vasiliev, D. Lossouarn, C. Romestant, A. Alexandre, Y. Bertin, Y. Piatsiushyk, et al., Loop heat pipe for cooling of high-power electronic components, Int. J. Heat Mass Transfer 52 (1–2) (2009) 301–308.
[4] D. Cytrynowicz, P. Medis, S. Parimi, A. Shuja, H. Thurman Henderson, F.M. Gerner, The MEMS loop heat pipe based on coherent porous silicon—the modified system test structure, in: AIP Conference Proceedings, American Institute of Physics, 2004, pp. 164–173.
[5] V.G. Pastukhov, Y.F. Maydanik, Low-noise cooling system for PC on the base of loop heat pipes, in: Twenty-Second Annual IEEE Semiconductor Thermal Measurement and Management Symposium, IEEE, 2006, pp. 95–101.
[6] S. Wang, J. Huo, X. Zhang, Z. Lin, Experimental study on operating parameters of miniature loop heat pipe with flat evaporator, Appl. Therm. Eng. 40 (2012) 318–325.
[7] X. Zhang, J. Huo, S. Wang, Experimental investigation on temperature oscillation in a miniature loop heat pipe with flat evaporator, Exp. Therm. Fluid Sci. 37 (2012) 29–36.
[8] S. Hong, X. Zhang, S. Wang, Z. Zhang, Experiment study on heat transfer capability of an innovative gravity assisted ultra-thin looped heat pipe, Int. J. Therm. Sci. 95 (2015) 106–114.
[9] S. Hong, S. Wang, Z. Zhang, Multiple orientations research on heat transfer performances of Ultra-Thin Loop Heat Pipes with different evaporator structures, Int. J. Heat Mass Transfer 98 (2016) 415–425.
[10] Y. Aono, N. Watanabe, A. Ueno, H. Nagano, Development of a loop heat pipe with kW-class heat transport capability, Appl. Therm. Eng. 183 (2021) 116169.
[11] M. Hashimoto, Y. Akizuki, K. Sato, A. Ueno, H. Nagano, Proposal, transient model, and experimental verification of loop heat pipe as heating device for electric-vehicle batteries, Appl. Therm. Eng. 211 (2022) 118432.
[12] M. Bernagozzi, A. Georgoulas, N. Miche, C. Rouaud, M. Marengo, Novel battery thermal management system for electric vehicles with a loop heat pipe and graphite sheet inserts, Appl. Therm. Eng. 194 (2021) 117061.
[13] N. Phan, Y. Saito, N. Katayama, H. Nagano, Operating characteristics of a dual flat-evaporator loop heat pipe for single heat source cooling in any orientation, Int. J. Heat Mass Transfer 172 (2021) 121146.
[14] Y. Qu, S. Qiao, D. Zhou, Steady-state modelling of dual-evaporator loop heat pipe, Appl. Therm. Eng. 193 (2021) 116933.
[15] Y. Qu, S. Wang, Y. Tian, A review of thermal performance in multiple evaporators loop heat pipe, Appl. Therm. Eng. 143 (2018) 209–224.
[16] A. Amhar, N. Putra, Development and testing multiple evaporator loop heat pipe utilizing three way T port valve, AIP Conf. Proc. 2255 (1) (2020) 070024.
[17] X. Chang, H. Nagano, Mathematical modeling of multiple evaporators/condensers loop heat pipe operation with flow regulator under various operating conditions, J. Therm. Sci. Technol. 10 (2) (2015). JTST0021-JTST0021.
[18] B. Chen, Z. Liu, W. Liu, J. Yang, H. Li, D. Wang, Operational characteristics of two biporous wicks used in loop heat pipe with flat evaporator, Int. J. Heat Mass Transfer 55 (7–8) (2012) 2204–2207.
[19] Z. Liu, D. Wang, C. Jiang, J. Yang, W. Liu, Experimental study on loop heat pipe with two-wick flat evaporator, Int. J. Therm. Sci. 94 (2015) 9–17.
[20] D. Wang, Z. Liu, S. He, J. Yang, W. Liu, Operational characteristics of a loop heat pipe with a flat evaporator and two primary biporous wicks, Int. J. Heat Mass Transfer 89 (2015) 33–41.
[21] S. He, Z. Liu, D. Wang, W. Liu, J. Yang, Effect of different charge ratios on transient performance of a flat type of the LHP with a shared compensation chamber, Int. J. Heat Mass Transfer 138 (2019) 1075–1081.